ChemInform Abstract: Thermoelectric Transport in Cu7PSe6 with High Copper Ionic Mobility.

ARTICLE *in* JOURNAL OF THE AMERICAN CHEMICAL SOCIETY · JULY 2014

Impact Factor: 12.11 · DOI: 10.1021/ja5056092 · Source: PubMed

JACS
JOURNAL OF THE AMERICAN CHEMICAL SOCIETY
Article
pubs.acs.org/JACS

Thermoelectric Transport in Cu_7PSe_6 with High Copper Ionic Mobility

Kai S. Weldert,[†,‡] Wolfgang G. Zeier,[§] Tristan W. Day,[§] Martin Panthöfer,[†] G. Jeffrey Snyder,*[,§] and Wolfgang Tremel*[,†]

[†]Institut für Anorganische Chemie und Analytische Chemie der Johannes Gutenberg-Universität, Duesbergweg 10-14, D-55128 Mainz, Germany

[‡]Graduate School Materials Science in Mainz, Johannes Gutenberg-Universität, Staudingerweg 9, 55128 Mainz, Germany

[§]Department of Applied Physics and Material Science, California Institute of Technology, Pasadena, California 91125, United States

ABSTRACT: Building on the good thermoelectric performances of binary superionic compounds like Cu_2Se, Ag_2Se and Cu_2S, a better and more detailed understanding of phonon-liquid electron-crystal (PLEC) thermoelectric materials is desirable. In this work we present the thermoelectric transport properties of the compound Cu_7PSe_6 as the first representative of the class of argyrodite-type ion conducting thermoelectrics. With a huge variety of possible compositions and high ionic conductivity even at room temperature, the argyrodites represent a very good model system to study structure–property relationships for PLEC thermoelectric materials. We particularly highlight the extraordinary low thermal conductivity of Cu_7PSe_6 below the glass limit, which can be associated with the molten copper sublattice leading to a softening of phonon modes.

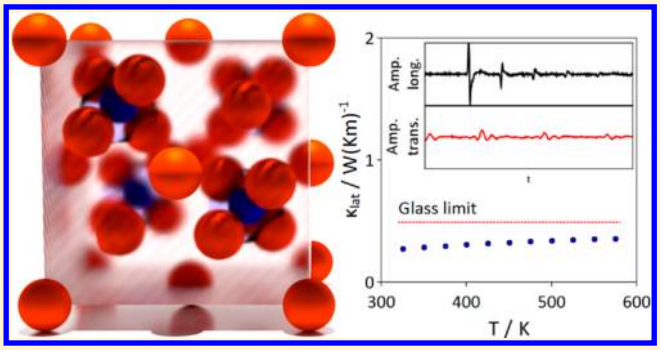

INTRODUCTION

In order to avoid a serious energy crisis in the future, alternative energy sources are required and new, powerful approaches have to be explored to use current energy technologies more efficiently. In fact, thermoelectric devices can be very useful in that regard since they are capable of generating electric power directly from a temperature gradient, for example, between a waste heat source and ambient temperatures. In order to increase the scope of applications for thermoelectric devices, it is essential to explore new materials and to improve thermoelectric efficiencies. The efficiency of a thermoelectric material is governed by its thermoelectric figure of merit $zT = S^2(\rho\kappa)^{-1}T$, with the Seebeck coefficient S, the electrical resistivity ρ, the thermal conductivity κ and the absolute temperature T. The thermal conductivity itself is a sum of an electronic contribution κ_{el} and a lattice contribution κ_{lat}. An optimal efficiency can be achieved for materials with a high electric and a low thermal conductivity in combination with a high Seebeck coefficient. As these parameters depend strongly on the electronic and phononic transport properties of the material, it is not possible to tune them independently. According to the "phonon-glass electron crystal" concept, a good thermoelectric material requires an optimized charge carrier concentration and a low lattice thermal conductivity.[1,2]

In recent years, new classes of thermoelectric materials have been discovered fulfilling this concept in various ways, usually by merging two fractional or structural units responsible for the electronic and thermal properties. In this context special attention was paid to skutterudites[3−5] and chalcopyrite-like structures.[6,7] The latter, for example, are doped ternary chalcogenides consisting of an electrically conducting tetrahedral network in combination with a highly disordered structure. These point defects act as phonon scattering centers, reducing the lattice thermal conductivity.[7] Here, high zT values could be achieved for doped samples, despite the fact that these compounds are wide band gap materials with a low mobility of the charge carriers.[6] In recent publications the concept of using two structural units, one responsible for suitable electronic properties and the other for lattice thermal conductivity has been applied to superionic compounds like Cu_2Se, Cu_2S, Ag_2Se and related compounds.[8−11] In this context the concept of phonon-liquid electron-crystal (PLEC) thermoelectrics has been introduced as an extension of the phonon-glass electron-crystal concept, because these materials are usually built up of a very simple anion network, in which the cations are highly disordered with liquid-like mobility, leading to very low lattice thermal conductivities.[12,13]

Inspired by the promising thermoelectric properties of these simple binary compounds, here we present the thermoelectric properties of Cu_7PSe_6, a member of the argyrodite family with the general formula $A^{x+}_{12-y/x}B^{y+}Q^{2-}_6$ for ternary compounds, which is a class of more complex ionic conductors. The ionic conductivity results from positional disorder characterized by a coalescence of the different A-cation positions through voids into a molten A-cation sublattice, while the B-cations and the

Received: June 4, 2014
Published: July 24, 2014

   dx.doi.org/10.1021/ja5056092 | J. Am. Chem. Soc. 2014, 136, 12035−12040

anions remain stationary. Partially ordered and disordered modifications can also be found.[14−16] Cu_7PSe_6 and related argyrodite compounds have already been investigated in the past with a focus on understanding their ionic conductivity.[17−19] Highly disordered modifications of lithium argyrodites with high ionic conductivities are considered as solid electrolytes for all solid state batteries.[20,21] However, a characterization of the thermoelectric properties of Argyrodite-type compounds has not yet been carried out. Due to a huge variety of compositions, which can even be increased by varying the oxidation states leading to both ternary and quaternary compounds, the argyrodites provide a huge playground for the investigation of structure−property relationships, making this class of materials a well-suited model system for phonon-liquid electron-crystal thermoelectric materials.[22,23]

The crystal structure of Cu_7PSe_6 has been investigated in previous publications.[15,16,24,25] As a representative example of the argyrodite structure type and the structure type variants derived from this, Cu_7PSe_6 can be described as a cubic close-packing of Se^{2-} anions, with additional Se^{2-} and tetrahedral $[PSe_4]^{3-}$ units alternately occupying the tetrahedral voids, which is illustrated in Figure 1. This anionic framework is

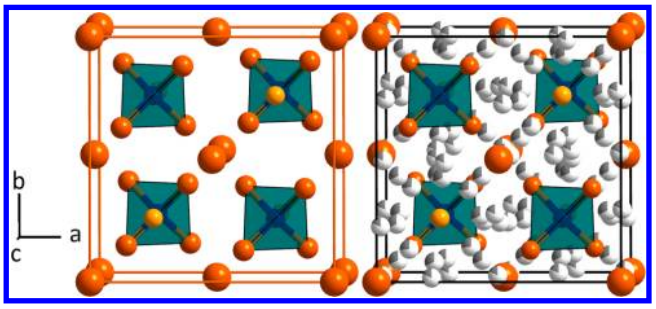

Figure 1. Crystal structure of the fully disordered, face-center-cubic ($F\bar{4}3m$) modification of Cu_7PSe_6. Selenium is shown in orange and phosphorus in blue. The orange bordered selection is an illustration of the $[PSe_6]^{7-}$ anion sublattice. Se^{2-} ions form a cubic close packed framework with Se^{2-} and tetrahedral $[PSe_4]^{3-}$ units alternately occupying the tetrahedral voids. Partly filled spheres in the black bordered selection (right) represent the Cu^+ cations, which are delocalized throughout the structure. The degree of filling represents the site occupancy according to Gaudin et al., who also showed images of the joint probability density function (jpdf) illustrating the high disorder of the copper ions.[15]

stuffed with copper cations, capable of moving along preferential diffusion paths within the $[PSe_6]$-framework at higher temperatures. Cu_7PSe_6 exhibits two structural phase transitions.[15,16] At temperatures above 320 K, Cu_7PSe_6 crystallizes in a face-centered-cubic structure ($F\bar{4}3m$) with a fully disordered A-cation sublattice. A partial localization of the Cu^+ ions occurs below 320 K, resulting in a cubic primitive structure ($P2_13$), whereby the partial ordering occurs at the highest probability density sites of the high-temperature phase diffusion paths. Below 250 K a second phase transformation occurs where all cations preferably occupy the most stable sites along the diffusion paths resulting in a complete ordering of the copper atoms.[15]

In this work we describe the synthesis and chemical characterization of Cu_7PSe_6 as well as the characterization of the thermoelectric transport properties, including Seebeck coefficient, electrical resistivity and thermal conductivity. Simultaneous measurements of electrical resistivity and Hall coefficients provided additional information on the electrical transport. Speed of sound measurements were performed in order to estimate the Debye temperature and the minimal lattice contribution to the thermal conductivity. The obtained data are compared with those of the closely related superionic thermoelectric material Cu2Se in order to obtain a deeper understanding of the thermoelectric transport in ionic conductors within the phonon-liquid electron-crystal concept.

EXPERIMENTAL SECTION

Synthesis. Bulk samples of polycrystalline Cu_7PSe_6 were prepared by melting and annealing techniques using elemental powders of Cu (Alfa Aesar, 99.999%) and Se (Alfa Aesar, 99.999%), as well as P pieces (Alfa Aesar, 99.999%). In order to ensure the absence of copper oxides in the reaction mixture the copper powder was heated for several hours to 525 K under N_2/H_2 (95:5) flow in a tube furnace using a corundum boat as the reaction vessel. Phase purity of the starting materials was verified by X-ray diffraction and all synthetic procedures were carried out in a N_2 drybox. In order to ensure completely dry conditions, the synthesis was performed in evacuated quartz ampules, which were dried at 1073 K under dynamic vacuum for several hours before usage. For the synthesis of Cu_7PSe_6 the starting elements were thoroughly ground, sealed in quartz ampules and heated to 1323 K for 3 h. The obtained chunks were crushed, ground to a fine powder, sealed in quartz ampules again, and reannealed at 773 K for 72 h. The second annealing step was necessary to prevent the formation of the binary byproduct. All procedures were carried out in horizontal tube furnaces with heating and cooling rates of 5 K/min. The obtained powders were hand ground and consolidated into 1−1.5 mm thick, 10 mm diameter pellets at 473 K for 24 h under a force of 50−75 kN by hot pressing in steel dies. The resulting discs are extremely brittle and have more than 95% theoretical density, determined from the geometric densities.

Measurements. X-ray diffraction experiments were performed on a Siemens D5000 powder diffractometer equipped with a Braun M50 position-sensitive detector, Ge (220) monochromator, and Cu Kα radiation, with a step size of 0.0078°. Rietveld refinements were performed with TOPAS Academic V4.1 applying the fundamental parameter approach.[26] As structure model the crystallographic data from Gaudin et al.[15] were used. Simultaneous thermogravimetry and differential thermal analysis (TG-DTA) have been performed with a Netzsch STA 449 F3 Jupiter device between room temperature and 875 at 10 K/min, under argon flow, in order to elucidate phase stability at high temperatures.

The thermal diffusivity α was measured with a Netzsch laser flash diffusivity instrument (LFA 457) under continuous argon flow. In order to maximize the emissivity, samples were spray-coated with a thin layer of graphite before the measurement. Thermal conductivity was determined via $\kappa = \alpha C_p d$ with the heat capacity C_p and the geometric density d. C_p was estimated using the Dulong-Petit approximation ($C_p = 3k_B$ per atom), and theoretical densities were calculated from the molar mass and the refined lattice parameters. Electrical transport was characterized via measurements of the Seebeck coefficient, Hall coefficient and electrical resistivity. Electrical resistivity and Hall coefficients were measured simultaneously using the van der Pauw technique with pressure-assisted contacts under dynamic vacuum.[27] The Seebeck coefficient was calculated from the slope of the voltage versus temperature gradient measurements from chromel-Nb thermocouples under dynamic vacuum with a maximum ΔT of 7.5 K for all temperatures.[28] Speed of sound measurements were performed at room temperature to extract the longitudinal and transverse sound velocities, respectively. The data were obtained by use of a Panametrics NDT 5800 pulser/receiver head; the response was recorded with a Tektronix TDS 1012 digital oscilloscope. Honey was used as a couplant between the sample and the ultrasonic transducer.

The reported data have been obtained using the same pellet in order to correlate the measured properties. Each measurement has been carried out at least two times on the same pellet, and several

dx.doi.org/10.1021/ja5056092 | J. Am. Chem. Soc. 2014, 136, 12035−12040

samples were measured, in order to ensure that the measured data is reproducible with respect to temperature cycling up to 575 K. Measurement data include the data collected during heating and cooling.

RESULTS AND DISCUSSION

Chemical Characterization. The thermoelectric properties of argyrodite-type compounds have not been investigated yet, and therefore phase purity of the measured samples is very important. Even small amounts of impurities can have a huge influence on the electronic and thermal properties of a material, for example through enhanced phonon scattering due to nanosized impurities on grain boundaries.[29] Samples of Cu_7PSe_6 were checked for phase purity via X-ray powder diffraction, and all reflections could be indexed to the simple-cubic (space group $P2_13$) Cu_7PSe_6 phase. No secondary phases were observed (Figure 2). With the unit cell parameter of a = 10.1057(8) Å, R_{wp} = 6.221% and GoF = 1.268, the calculated data are in very good agreement with the lattice parameters reported by Kuhs et al., displaying a high purity of the prepared samples.[24] The isotropic thermal displacement parameters for copper were significantly higher than the parameters for selenium or phosphorus, which reflects the high mobility of the copper ions at room temperature. TGA/DSC analysis shows an exothermic event at around 325 K, representing the phase transition from the partially ordered, cubic primitive phase to the disordered face-centered-cubic phase. A small mass loss of about 0.5% could be observed at temperatures between 625 and 875 K probably associated with sample decomposition; therefore the following measurements of the thermoelectric transport properties of Cu_7PSe_6 were carried out only up to 575 K.

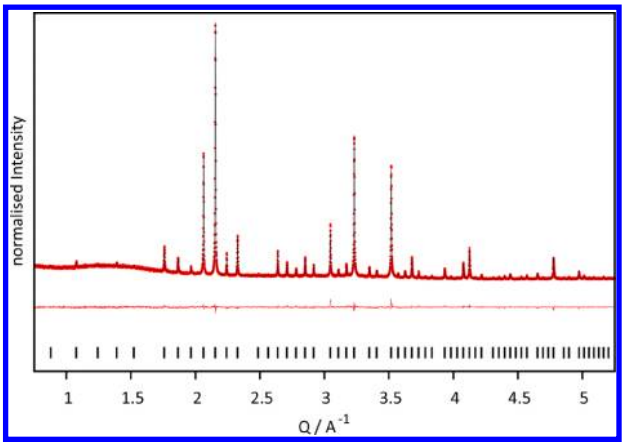

Figure 2. X-ray powder diffraction data for Cu_7PSe_6 (red dots), including profile fit (black solid line) and profile difference (red solid line) from the corresponding Rietveld refinement. All reflections could be indexed to the simple-cubic Cu_7PSe_6 phase with a = 10.1057(8) Å, R_{wp} = 6.221% and GoF = 1.268. No side phases were observed using standard laboratory X-ray diffraction data.

Electronic Transport Properties. The temperature dependent electrical resistivity of Cu_7PSe_6 is shown in Figure 3a. In the temperature region between 325 and 425 K a strong decrease of the electrical resistivity was observed, which might be related to the phase transition from the partially cation ordered to the fully disordered high temperature phase with an increasing amount of mobile copper ions.[15,19] A rate-dependent hysteretic-like behavior was observed between the heating and cooling data. This is possibly due to the cation disordering during the heating process and the cation ordering during the cooling process, which seems to appear gradually over a certain temperature range. Above 425 K this hysteresis disappears and the resistivity decreases with increasing temperature, as expected for a semiconductor. In this case the temperature dependence of the conductivity is governed by an Arrhenius-like, thermally activated process across the band gap which can be described through $\sigma = A \exp(-E_a/(2k_BT))$, where σ is the electric conductivity, A is a constant, E_a is the activation energy and k_B the Boltzmann constant. An Arrhenius plot of the data from 425 to 575 K is shown in the inset of Figure 3a. The calculated activation energy of 0.28 ± 0.01 eV is larger compared to the value of 0.17 eV for the high temperature modification and 0.22 eV for the low temperature modifications reported by Beeken et al.[19] However, the activation energies are in good agreement since the absolute values are very small. Temperature dependent Hall measurements were performed in order to obtain Hall carrier mobilities μ_H and Hall carrier concentrations n_H. The Hall carrier mobilities are very small and positive (Figure 3b), which might be expected for an ionic conducting material. The huge degree of disorder in the structure, which is correlated to the ionic conducting nature of this compound, leads to trapping of electronic states at the Fermi energy.[30] The positive values indicate that holes are the major charge carriers resulting from intrinsic defects, possibly induced by slight losses of selenium or phosphorus during the

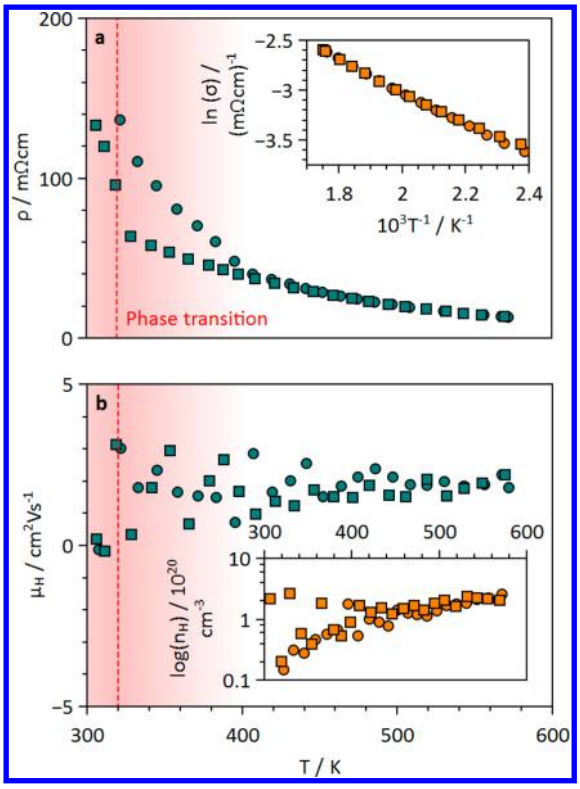

Figure 3. Temperature dependences of the electrical resistivity ρ with Arrhenius plot (a), as well as Hall mobility μ_H and Hall carrier concentration n_H (b) of Cu_7PSe_6. Circles represent heating data, squares represent cooling data. A temperature range of 80 K is highlighted in red around the phase transition of Cu_7PSe_6 (red dashed line), where the rate dependent hysteretic like behavior can be observed in the resistivity data. Cu_7PSe_6 illustrates semiconducting behavior with an activation energy of 0.28 ± 0.01 eV, showing extrinsic hole transport as a result of intrinsic defects.

dx.doi.org/10.1021/ja5056092 | J. Am. Chem. Soc. 2014, 136, 12035−12040

synthesis. Despite a slight decrease of n_H in the temperature range of the phase transition, which could be attributed to an additional increase of disorder, no significant temperature dependence could be observed for the Hall mobilities. As a consequence, no general statement can be made in relation to the scattering mechanism.[31] The Hall carrier concentration n_H increases significantly with temperature (see inset Figure 3b.) in the temperature region of the structural phase transition from the partial cation disordered simple cubic phase to the fully cation-disordered phase, which is consistent with the decreasing activation energy.[17] After the phase transformation the carrier concentration increases slightly, which can be attributed to the contribution of a growing number of holes, resulting from intrinsic defects in the material.

The temperature dependence of the Seebeck coefficient is shown in Figure 4; the Seebeck coefficient increases from about

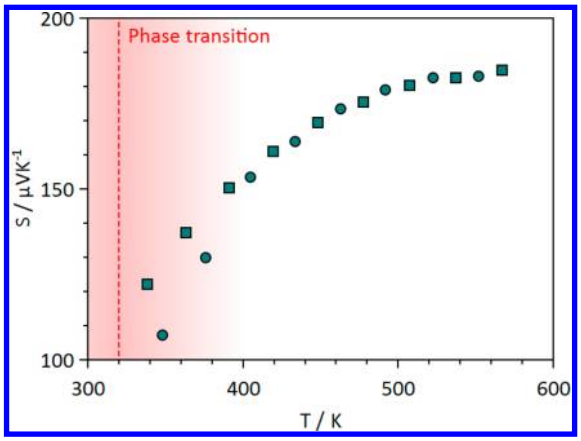

Figure 4. Temperature dependence of the Seebeck coefficient *S*. Circles represent heating data, squares represent cooling data. The Seebeck coefficient is positive and increases with temperature without reaching a maximum, which is consistent with the electrical resistivity and Hall data.

+40 μV/K at room temperature to +175 μV/K at 575 K. This increase in the thermopower indicates extrinsic hole transport, which is consistent with the resistivity and Hall data. Intrinsic conduction caused by thermal excitation of carriers is not the main contributor in the observed temperature range, which would result in a peak Seebeck coefficient followed by decline. This observation is consistent with the calculated activation energy of 0.28 eV.

Thermal Transport Properties. The total thermal conductivity of Cu_7PSe_6 increases slightly from 0.3 $W(Km)^{-1}$ to 0.4 $W(Km)^{-1}$ in the measured temperature range (see Figure 5). Cu_7PSe_6 has not yet been optimized with respect to the electronic properties, therefore, the electrical resistivities are still high compared to typical resistivities in related thermoelectric materials. Due to this, the electronic contribution to the total thermal conductivity is negligible at lower temperatures and below 10% at higher temperatures.[12,13] The electronic contribution to the thermal conductivity has been estimated, using the Wiedemann–Franz law ($\kappa_{el} = LT\rho^{-1}$), with $L = 1.5 \cdot 10^{-8}$ $W\Omega K^{-2}$ for nondegenerate materials.[31] The obtained values of the lattice contribution to the thermal conductivities are significantly lower than the lattice thermal conductivities of most of the state of the art thermoelectric materials, which usually are above 1 $W(Km)^{-1}$. Further, almost no temperature dependence of the thermal conductivity can be seen over the

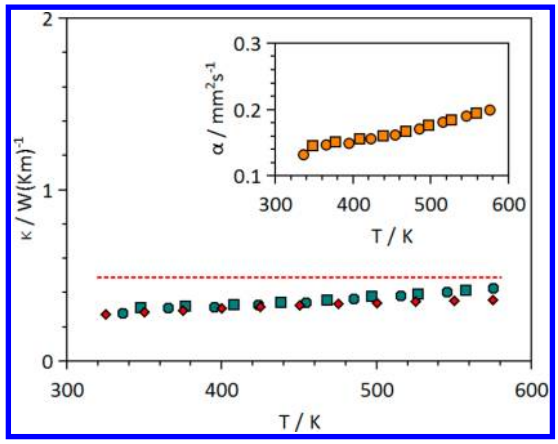

Figure 5. Temperature dependences of the thermal conductivity κ with related thermal diffusivity α (inset). The cyan circles and squares represent the total thermal conductivity κ (heating and cooling). Red diamonds show the lattice thermal conductivity κ_{lat}, which has been estimated from the Wiedemann–Franz law. The glassy limit of the lattice thermal conductivity κ_{min} has been determined by Cahill's formulation and is represented by the red dotted line, which lies above the measured values for κ.

investigated temperature range. In contrast, most crystalline solid materials exhibit strong temperature dependence of their lattice thermal conductivity, usually following a T^{-1} trend at high temperatures, indicating Umklapp-scattering to be the major scattering mechanism.[32]

However, highly disordered materials like glasses often show different temperature behaviors for the thermal conductivity.[33] For the argyrodite Cu_7PSe_6, the ionic conducting character leads to a very high positional disorder resulting in very low, temperature independent lattice thermal conductivities. The melt-like behavior of the mobile Cu ions is responsible for a very short phonon mean free path, which results in κ_{lat} values in range of the glass limit. Furthermore, the low thermal conductivity can be attributed to the large unit cell of Cu_7PSe_6, composed of 56 atoms. This leads to a larger number of optical modes with low group velocities, which contribute less to the thermal conductivity.[34] The more complex structure might explain the lower lattice thermal conductivity of Cu_7PSe_6 compared to the related superionic conductor Cu_2Se, which has a lattice thermal conductivity around 0.4–0.6 $W(mK)^{-1}$ at high temperatures.[12]

Ultrasonic measurements of longitudinal and transverse sound velocities were performed at room temperature to estimate the Debye temperature Θ_D and the minimal thermal conductivity κ_{min}. The longitudinal and transversal speed of sounds were found to be $v_l = 3580$ ms^{-1} and $v_t = 1870$ ms^{-1}, respectively. With these, the Debye temperature was estimated to be 215 K via[35]

$$\Theta_D = \frac{V_m \hbar}{k_B}\left(\frac{6\pi^2}{V}\right)^{1/3}$$

where V is the average volume per atom calculated from the refined lattice parameters, and v_m is the average speed of sound determined by the formula of Anderson for an isotropic material.[34]

$$V_m = \left(\frac{1}{3}\left[\frac{2}{v_t^3} + \frac{1}{v_l^3}\right]\right)^{-1/3}$$

dx.doi.org/10.1021/ja5056092 | J. Am. Chem. Soc. 2014, 136, 12035–12040

The low Debye temperature is typical for a material with a less rigid crystal structure. According to Cahill's formulation, the glassy limit for the thermal conductivity κ_{min} can be estimated.[31,36] The high temperature limit for the minimum lattice thermal conductivity is

$$k_{min} = \frac{1}{2}\left(\frac{\pi}{6}\right)^{1/3} k_B V^{-2/3}(2v_t + v_l)$$

leading to a value of κ_{min} = 0.49 W(Km)$^{-1}$.[31] Interestingly, the calculated value of κ_{min} is higher than the measured lattice thermal conductivity over the whole temperature range, which is in accordance with observations made on the superionic compounds Cu_2Se and Cu_2S.[12,13]

Cahill's formulation of the glass limit employs a summation over all sound modes with their associated speeds of sound. Removing a fraction of the heat propagating modes will lead to a lower value of κ_{min}. For instance, in order to bring the κ_{min} calculated here for Cu_7PSe_6 in the range of the measured value of κ_{lat}, half of the shear modes would have to be removed.[13] Some examples for materials with thermal conductivities below the predicted minimal limit are known in disordered layered materials, which is attributed to a localization of lattice vibrations, making them unable to contribute to heat conduction.[37] In other words, these low lattice thermal conductivities may be due to shear modes, which do not propagate through the lattice. Therefore, Cu_7PSe_6 might show lattice thermal transport behavior close to a real liquid, where shear modes do not propagate at all. The assumption of an influence of the high-mobility cations in superionic compounds on transverse lattice modes can be supported by the comparison of the longitudinal and transverse speed of sound data of Cu_7PSe_6 and Cu_2Se. The longitudinal speed of sound of Cu_7PSe_6 (v_l = 3580 ms^{-1}) is a little higher compared to Cu_2Se with v_l = 3350 ms^{-1}, while the transverse speed of sound is significantly lower (v_t = 2320 ms^{-1} for Cu_2Se and v_t = 1870 ms^{-1} for Cu_7PSe_6). While both speed of sound measurements were performed at room temperature, Cu_7PSe_6 is ion-conducting during the measurement, whereas Cu_2Se is superionic only above 400 K.[12] The much lower transverse speed of sound is an indication for a significant softening of shear modes due to the melt-like copper sub lattice. It has to be taken in consideration that Cahill's formulation is based on assumptions which might not hold for superionic materials. Further investigations will be performed to provide a more detailed understanding of the extraordinarily low thermal conductivities in argyrodite-type ionic conducting compounds.

Figure of Merit. The maximum zT of 0.35 at 575 K is very promising (Figure 6), as exclusively a nominally valence precise compound was studied in this work. Similar to the related binary superionic compounds Cu_2Se and Cu_2S, the power factor needs to be optimized via substitution in order to obtain higher values for the figure of merit in Cu_7PSe_6 or related compounds.[12,13]

SUMMARY

We have synthesized the copper ion conducting argyrodite Cu_7PSe_6 and characterized its thermoelectric transport properties. Very high copper ionic conductivities even at low temperatures make argyrodite-type compounds an excellent model system to study phonon-liquid electron-crystal thermoelectrics. Cu_7PSe_6 shows potential as a thermoelectric material due to an extraordinarily low thermal conductivity, which arises from a high structural disorder and a liquid-like behavior of the material. The "molten" Cu-sublattice leads to a softening of phonon modes, ultimately affecting the thermal transport. We believe this class of materials, the argyrodites, to be a new and promising approach to novel thermoelectric materials within the phonon-liquid electron-crystal concept.

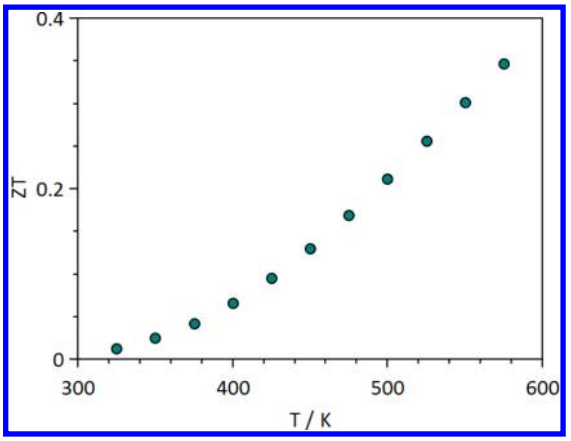

Figure 6. Temperature dependence of the dimensionless figure-of-merit zT.

AUTHOR INFORMATION

Corresponding Authors

jsnyder@caltech.edu

tremel@uni-mainz.de

Notes

The authors declare no competing financial interest.

ACKNOWLEDGMENTS

Financial support through the Excellence Initiative (DFG/GSC 266) is acknowledged by K.W. We acknowledge support from the DFG priority program SPP1386 "Nanostructured Thermoelectrics". T. W. Day and G. J. Snyder acknowledge support from the U.S. Air Force Office of Scientific Research. We gratefully thank David Brown (CalTech) for fruitful discussions.

REFERENCES

(1) Bell, L. E. *Science* **2008**, *321*, 1457−1461.
(2) Slack, G. A. In *CRC Handbook Of Thermoelectrics*; Rowe, D. M., Ed.; CRC Press: Boca Raton, FL, 1995.
(3) Sharp, J. W.; Jones, E. C.; Williams, R. K.; Martin, P. M.; Sales, B. C. *J. Appl. Phys.* **1995**, *78*, 1013.
(4) Sales, B.; Mandrus, D.; Williams, R. *Science* **1996**, *272*, 1325−1328.
(5) Nolas, G.; Morelli, D. *Annu. Rev. Mater.* **1999**, 89−116.
(6) Liu, M.-L.; Chen, I.-W.; Huang, F.-Q.; Chen, L.-D. *Adv. Mater.* **2009**, *21*, 3808−3812.
(7) Zeier, W. G.; Pei, Y.; Pomrehn, G.; Day, T.; Heinz, N.; Heinrich, C. P.; Snyder, G. J.; Tremel, W. *J. Am. Chem. Soc.* **2013**, *135*, 726−732.
(8) Liu, H.; Shi, X.; Kirkham, M.; Wang, H.; Li, Q.; Uher, C.; Zhang, W.; Chen, L. *Mater. Lett.* **2013**, *93*, 121−124.
(9) Ferhat, M.; Nagao, J. *J. Appl. Phys.* **2000**, *88*, 813.
(10) Day, T.; Drymiotis, F.; Zhang, T.; Rhodes, D.; Shi, X.; Chen, L.; Snyder, G. J. *J. Mater. Chem. C* **2013**, *1*, 7568.
(11) Drymiotis, F.; Day, T. W.; Brown, D. R.; Heinz, N. a.; Jeffrey Snyder, G. *Appl. Phys. Lett.* **2013**, *103*, 143906.
(12) Liu, H.; Shi, X.; Xu, F.; Zhang, L.; Zhang, W.; Chen, L.; Li, Q.; Uher, C.; Day, T.; Snyder, G. J. *Nat. Mater.* **2012**, *11*, 422−425.

(13) He, Y.; Day, T.; Zhang, T.; Liu, H.; Shi, X.; Chen, L.; Snyder, G. J. *Adv. Mater.* **2014**, *26*, 3974−3978.
(14) Evain, M.; Gaudin, E.; Boucher, F.; Petricek, V.; Taulelle, F. *Acta Crystallogr., Sect. B: Struct. Sci.* **1998**, *54*, 376−383.
(15) Gaudin, E.; Boucher, F.; Petricek, V.; Taulelle, F.; Evain, M. *Acta Crystallogr., Sect. B: Struct. Sci.* **2000**, *56*, 402−408.
(16) Gaudin, E.; Petricek, V.; Boucher, F.; Taulelle, F.; Evain, M. *Acta Crystallogr., Sect. B: Struct. Sci.* **2000**, *56*, 972−979.
(17) Beeken, R. B.; Driessen, C. R.; Hinaus, B. M.; Pawlisch, D. E. *Solid State Ionics* **2008**, *179*, 1058−1060.
(18) Beeken, R. B.; Driessen, C. R.; Wilson, L. a. *J. Phys. Chem. Solids* **2009**, *70*, 1181−1184.
(19) Beeken, R. B.; Hinaus, B. M. *J. Phys. Chem. Solids* **2011**, *72*, 1081−1084.
(20) Deiseroth, H.-J.; Kong, S.-T.; Eckert, H.; Vannahme, J.; Reiner, C.; Zaiss, T.; Schlosser, M. *Angew. Chem., Int. Ed. Engl.* **2008**, *47*, 755−758.
(21) Rao, R. P.; Adams, S. *Phys. Status Solidi* **2011**, *208*, 1804−1807.
(22) Nilges, T.; Pfitzner, A. *Z. Kristallogr.* **2005**, *220*, 281−294.
(23) Hahn, H.; Schulze, H.; Sechser, L. *Naturwissenschaften* **1965**, *52*, 451.
(24) Kuhs, W. F.; Schulte-Kellinghaus, M.; Krämer, V.; Nitsche, R. *Z. Naturforsch.* **1977**, *32b*, 1100−1101.
(25) Kuhs, W. F.; Nitsche, R.; Scheunemann, K. *Mater. Res. Bull.* **1979**, *14*, 241−248.
(26) Coelho, A. *TOPAS*, Academic V4.1; Coelho Software: Brisbane, Australia, 2004.
(27) Borup, K. a; Toberer, E. S.; Zoltan, L. D.; Nakatsukasa, G.; Errico, M.; Fleurial, J.-P.; Iversen, B. B.; Snyder, G. J. *Rev. Sci. Instrum.* **2012**, *83*, 123902.
(28) Iwanaga, S.; Toberer, E. S.; LaLonde, A.; Snyder, G. J. *Rev. Sci. Instrum.* **2011**, *82*, 063905.
(29) Zeier, W. G.; LaLonde, A.; Gibbs, Z. M.; Heinrich, C. P.; Panthöfer, M.; Snyder, G. J.; Tremel, W. *J. Am. Chem. Soc.* **2012**, *134*, 7147−7154.
(30) Lee, P.; Ramakrishnan, T. *Rev. Mod. Phys.* **1985**, *57*, 287−337.
(31) May, A. F.; Snyder, G. J. In *Thermoelectrics Handbook: Thermoelectrics and Its Energy Harvesting*; Rowe, D. M., Ed.; CRC Press: Boca Raton, FL, 2012; Chapter 11.
(32) Slack, G. *Solid State Phys.* **1979**, *34*, 1−71.
(33) Zeller, R.; Pohl, R. *Phys. Rev. B: Solid State* **1971**, *4*, 2029−2041.
(34) Toberer, E. S.; Zevalkink, A.; Snyder, G. J. *J. Mater. Chem.* **2011**, *21*, 15843.
(35) Anderson, O. *J. Phys. Chem. Solids* **1963**, *24*, 909−917.
(36) Cahill, D.; Watson, S.; Pohl, R. *Phys. Rev. B: Condens. Matter Mater. Phys.* **1992**, *46*, 6131−6140.
(37) Chiritescu, C.; Cahill, D. G.; Nguyen, N.; Johnson, D.; Bodapati, A.; Keblinski, P.; Zschack, P. *Science* **2007**, *315*, 351−353.